

Dependence of fluid flows in an evaporating sessile droplet on the characteristics of the substrate

L.Yu. Barash^{1,2,a)}

¹⁾ *Landau Institute for Theoretical Physics,
142432 Chernogolovka, Russia*

²⁾ *Moscow Institute of Physics and Technology,
141700 Moscow, Russia
e-mail: ^{a)}barash@itp.ac.ru*

Temperature distributions and the corresponding vortex structures in an evaporating sessile droplet are obtained by performing detailed numerical calculations. A Marangoni convection induced by thermal conduction processes in the drop and the substrate is demonstrated to be able to result not only in a single vortex, but also in two or three vortices, depending on the ratio of substrate to fluid thermal conductivities, on the substrate thickness and the contact angle. The “phase diagrams” containing information on the number, orientation and spatial location of the vortices for quasistationary fluid flows are presented and analysed. The results obtained demonstrate that the fluid flow structure in evaporating droplets can be influenced in a controlled manner by selecting substrates with appropriate properties.

I. INTRODUCTION

A temperature variation along the liquid-vapor interface of an evaporating droplet can generate a thermocapillary flow inside the drop. The structure of the fluid flow in an evaporating droplet is of interest for a number of applications and has been intensively studied (see, for example, [1, 2] and references therein). The substrate properties also play an important role in the nanotechnology applications of the problem. One of the examples is self-assembly of superlattices of nanoparticles taking place during evaporation of colloidal solutions. It is known that substrate characteristics can strongly influence both the deposition patterns and the self-assembly process [3–8].

A sensitivity of Marangoni fluid flows to the droplet contact angle is known since Hu and Larson demonstrated that fluid circulation in the vortex can reverse its sign at a critical contact angle for a drop placed onto substrates with finite thicknesses [9]. It was originally observed and described by Ristenpart et al. that the circulation direction depends on the substrate to liquid ratio of the thermal conductivities [10]. Specifically, the authors found that the ratio determines the sign of the tangential component of the temperature gradient at the surface close to the contact line, and, therefore, it determines a direction of the circulation in that region. Assuming the key role of a small vicinity of the contact line in forming the circulation direction in a single vortex, the shape of the liquid-vapor interface in that small region was approximated as a plane, which is actually inappropriate since the three-phase contact line has finite radius of curvature. However, the conditions for the circulation sign change have been found within such framework. While the approach and predictions of Ref. [10] generally are qualitatively insightful and quite useful, the particular approximations made and the corresponding quantitative results obtained in [10] have not been justified by more accurate numerical calculations.

An alternative approach suggested by Xu et al. [11], focuses on a heat transfer in the immediate vicinity of the symmetry axis peering the apex. The change of sign of the tangential gradient of the temperature near the apex and, hence, the corresponding transition between the opposite circulation directions, taking place with a variation of the relative substrate-liquid thermal conductivity, has been identified by the authors under different conditions as compared to the results of [10]. Transition points at various contact angles obtained in [11] are much closer to the results of subsequent numerical calculations and are in agreement with the corresponding experimental data.

The above studies [9–11] assumed a monotonic temperature profile along the droplet surface, and, hence, a single-vortex fluid flow. However, such an assumption only partially explains the phenomenon. The thermal conduction processes throughout the droplet can generally result in a nonmonotonic spatial dependence of the surface temperature and in more complicated convection patterns inside a drop. In particular, either a single vortex or several vortices are formed in the droplet depending on the thermal conductivity of the substrate [12]. With varying the relative substrate-liquid thermal conductivity, transitions between regimes with different numbers of vortices and/or circulation directions take place. This has been described recently in more detail by Zhang et al. in [13], where the authors presented the “phase diagram” characterizing, for a fixed substrate thickness ($h_R = 0.1$ in units of contact line radius), the distribution of surface temperature in the k_R – θ plane, where k_R is ratio of substrate to fluid thermal conductivities and θ is contact angle.

The three regions in the k_R – θ plane have been demonstrated in [13]. In region I the surface temperature monotonically increases from the center to the edge of the droplet. In region III the surface temperature decreases monotonically

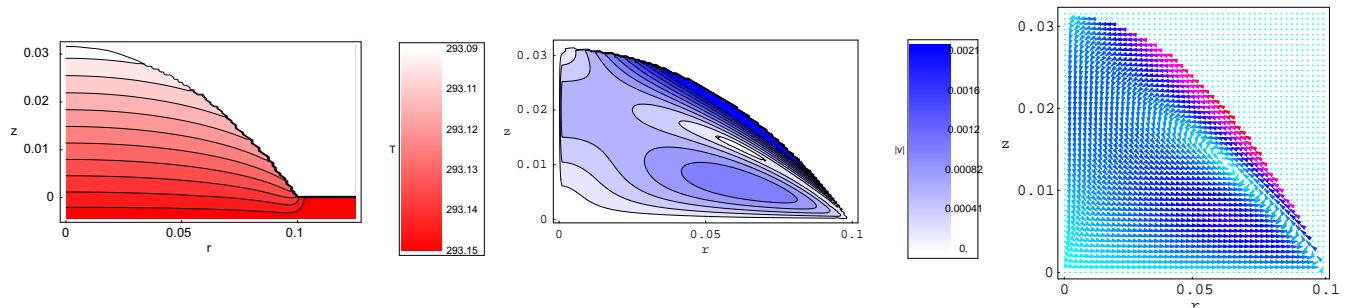
from the center to the edge of the droplet. Finally, in region II the temperature exhibits a nonmonotonic spatial dependence along the droplet surface. Naturally, regions I and III correspond to single-vortex states with opposite circulations of the fluid flows. In the present work we focus on the substructure of the region II. Specifying the number of the temperature extrema along the droplet surface, we find the subregions, which correspond to two or three vortices inside the droplet. We also identify the dependence of the borders between the subregions on the substrate thickness. The results obtained demonstrate that the vortex state structure in evaporating droplets of capillary size can be prepared in a controlled manner by selecting substrates with appropriate thermal conductivity and thickness.

II. RESULTS AND DISCUSSION

We have carried out the numerical simulation of the evaporation and fluid dynamics of droplets of capillary size and studied the dependence of the results on the characteristics of the substrate. The thermal conduction equation has been solved using the numerical method described in Appendix A, where the equations and the boundary conditions used are presented as well. The Navier-Stokes equations in the droplet region were solved using the numerical method of Ref. [14].

Figs. 1–5 demonstrate spatial temperature distributions both inside the droplet and the substrate, distributions of absolute value of the fluid velocity and vector field plots of the velocity. The parameter set used is taken for 1-hexanol and presented in Table I. Since 1-hexanol is weakly volatile liquid, the evaporation process is comparatively slow, and the corresponding inverse Stanton number $St^{-1} = \bar{u}R/\kappa$ is much smaller than unity for the droplets of relatively small size considered (here \bar{u} is a characteristic value of fluid velocity). Hence, the convective heat transfer is negligibly small. Also we consider the evaporation as a quasistationary process, which is realized when the transient time for heat transfer $t_{\text{heat}} = R(h_0 + h_S)/\kappa$, transient time for momentum transfer $t_{\text{mom}} = \rho R h_0/\eta$ and transient time for vapor phase mass transfer $t_{\text{mass}} = \rho_{\text{vap}}/\rho \cdot t_f$ are much smaller than the total drying time $t_f \approx 0.2\rho R h_0/(Du_s)$. Here h_0 is the droplet height and h_S is the substrate thickness. In addition, the droplet shape can be described with good accuracy within the spherical cap approximation when the capillary number $Ca = \eta\bar{u}/\sigma$ and the Bond number $Bo = \rho g h_0 R/(2\sigma \sin \theta)$ are much smaller than unity [14].

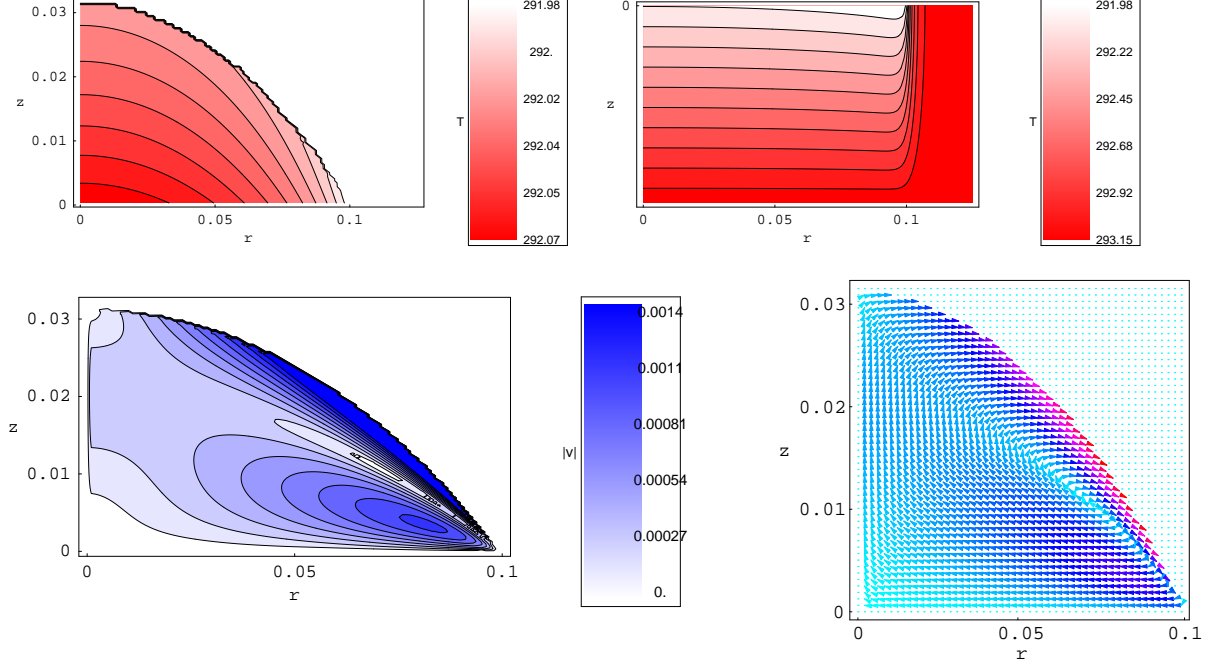
FIG. 1: Temperature distribution, distribution of absolute value of velocity and vector field plot of velocity for a droplet of 1-hexanol in a single-vortex regime obtained for $\theta = 35^\circ$, $k_R = 1$, $h_R = 0.05$.



Since driving forces for fluid convection are the Marangoni forces and $\partial\sigma/\partial T < 0$, the fluid usually flows from a surface region with higher temperature to that with lower temperature. Therefore, the single-vortex flow corresponds to a surface temperature, which monotonically increases with increasing the axial coordinate r (see Figs. 1,5). The reversed single-vortex flow (see Figs. 2,5) corresponds to a monotonically decreasing surface temperature dependence on r . The surface temperature, which induces a two-vortex or three-vortex flow, is found to be a nonmonotonic function of r with a single extremum (in addition to extrema at the apex and at the contact line) in the two-vortex case and with both maximal and minimal values in the three-vortex case (see Figs. 3–5). Fig. 5 shows surface temperature distributions for the droplets in Figs. 1–4.

The parameter regions of different types of surface temperature distribution are shown in Fig. 6 in the form of the “phase diagram” in the k_R – θ plane, taken for various values of the substrate thickness. One can see that the region II of a nonmonotonic spatial dependence of the surface temperature consists of two regions. One of them, II_2 , corresponds to the two-vortex flows, while another one, II_3 , corresponds to the flows with three vortices. Black curve in Fig. 6 corresponds to the change of sign of the tangential component of temperature gradient at the liquid-vapor interface near the contact line. Blue curve in Fig. 6 corresponds to the change of sign of the tangential component of temperature gradient at the liquid-vapor interface at the droplet apex. Red curve in Fig. 6 corresponds to the

FIG. 2: Temperature distribution inside the droplet and the substrate correspondingly, distribution of absolute value of velocity and vector field plot of velocity in a reversed single-vortex regime obtained for 1-hexanol, $\theta = 35^\circ$, $k_R = 0.01$, $h_R = 0.05$.



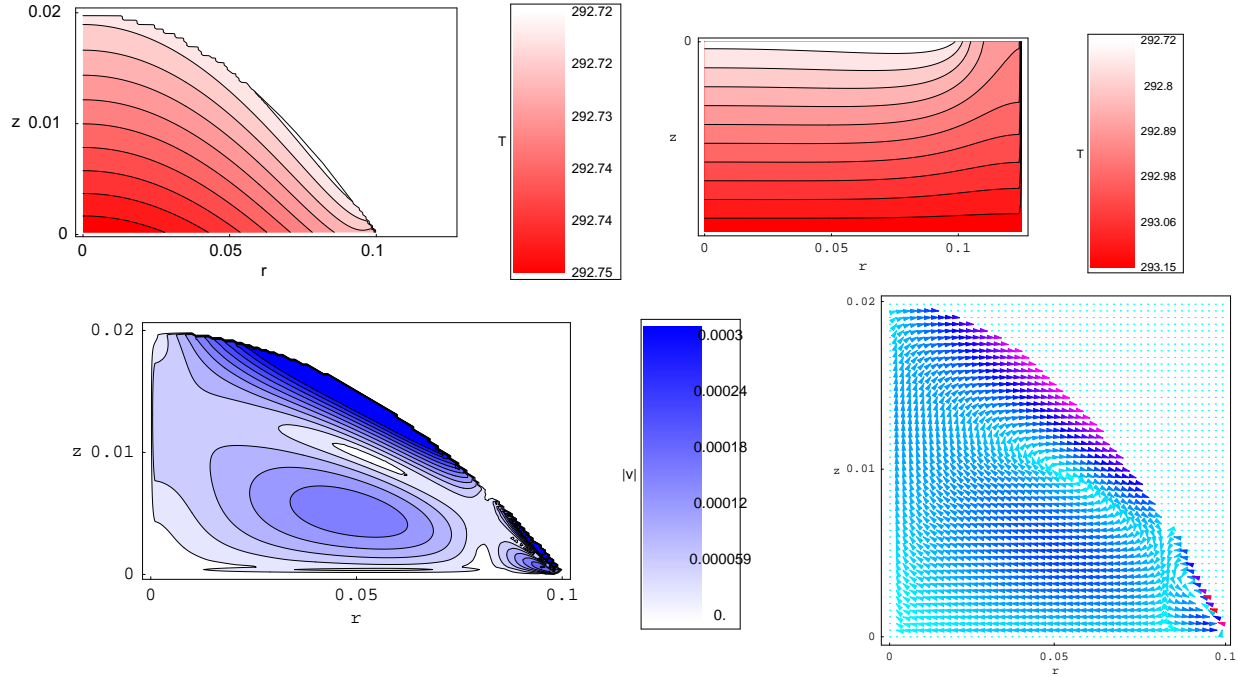
transition between a nonmonotonic dependence of surface temperature on r and a monotonically increasing surface temperature dependence on r .

The “phase diagram” shows that the regime of convection changes during the evaporation process when the contact angle diminishes. For example, when k_R is large, three vortices can appear at relatively small contact angles (see also [14]).

The main features of a “phase diagram” can be qualitatively understood as a result of matching the heat transfer through the solid-liquid interface and the vaporization heat, which flows through the liquid-vapor interface. When k_R is small, the vaporization heat is much stronger than the heat flow from the substrate. Since an inhomogeneous evaporation rate $J_s(r) = J_0(\theta)(1 - r^2/R^2)^{-\lambda(\theta)}$ has its minimum at the apex, the surface region near the apex should be warmer than at the contact line. Thus, $k_R \ll 1$ results in a monotonic decrease of the surface temperature with r , which corresponds to the reversed single-vortex regime, i.e., to the region III of the “phase diagram”. If, on the contrary, $k_R \gg 1$, then the heat flowing through the solid-liquid interface is much stronger than the vaporization heat flow. Therefore, the area of liquid-vapor interface close to the contact line is the warmest one due to adjacent highly conducting substrate. In this case the surface area close to the apex is colder as compared to other parts of the droplet. Thus, $k_R \gg 1$ results in a monotonic increase of the surface temperature with r , which corresponds to the single-vortex region I of the “phase diagram”. We also note that the increase of the nonuniform evaporation rate $J_s(r) = J_0(\theta)(1 - r^2/R^2)^{-\lambda(\theta)}$ near the contact line becomes more pronounced with decreasing the contact angle, since $\lambda(\theta) = 1/2 - \theta/\pi$. For this reason, at small contact angles the vaporization heat flow usually dominates near the contact line and results in the reversed single-vortex region III of the “phase diagram”. At large contact angles, the heat flow from the substrate has much more chances to dominate, and this results in the region I of the “phase diagram”.

We also study the dependence of the fluid flows on the thickness of the substrate. Fig. 6 shows the “phase diagram” obtained for different values of $h_R = h_S/R$. As seen in Fig. 6, with an increase of the substrate thickness, the subregion II_2 becomes dominating in the region II. Further increase of the substrate thickness results in shifting the regions I and II to larger contact angles. The blue curve in Fig. 6 is situated below the black curve at small values of h_R , while at larger values of h_R it is above the black curve. Therefore, the transition between the regions III and II_2 corresponds to the change of sign of the tangential component of the temperature gradient at the liquid-vapor interface either at the droplet apex (for small substrate thickness) or near the contact line (for larger substrate thickness). The transition between the regions II_2 and II_3 corresponds to the change of sign of the tangential component of the temperature gradient at the liquid-vapor interface either near the contact line (for small substrate thickness) or at the droplet apex (for larger substrate thickness). Fig. 7 shows the dependence of θ_{crit} on h_R for the transitions between the regions I,

FIG. 3: Temperature distribution inside the droplet and the substrate correspondingly, distribution of absolute value of velocity and vector field plot of velocity for a droplet of 1-hexanol in a two-vortex regime obtained for $\theta = 22.44^\circ$, $k_R = 0.2$, $h_R = 0.5$.



Π_2 , Π_3 and III. A behavior of critical angles as a function of h_R shown in Fig. 7 is, naturally, different in the region $h_R \lesssim 0.1$, where the blue curve is below the black curve in Fig. 6, and in the region $h_R \gtrsim 0.1$, where it is above the black curve.

III. CONCLUSION

The fluid flow structure in an evaporating sessile droplet of capillary size has been considered in disregarding the convective heat transfer, i.e., for relatively small and slowly evaporating droplets (when $St^{-1} = \bar{u}R/\kappa \ll 1$). It is shown that the region II of the “phase diagram” introduced in [13] consists of the two subregions Π_2 and Π_3 , where Π_2 corresponds to the flows with two vortices and Π_3 corresponds to the flows with three vortices. The transition between the regions III and Π_2 corresponds to the change of sign of the tangential component of the temperature gradient at the liquid-vapor interface either at the droplet apex (for small substrate thickness) or near the contact line (for larger substrate thickness). The transition between the regions Π_2 and Π_3 corresponds to the change of sign of the tangential component of the temperature gradient at the liquid-vapor interface either near the contact line (for small substrate thickness) or at the droplet apex (for larger substrate thickness). Further increase of the substrate thickness makes subregion Π_2 dominating in region II, and results in a shift of the regions I and II to larger contact angles.

Temperature distribution, fluid flow structure in the droplet and general form of a “phase diagram” can be qualitatively understood as a result of matching the heat transfer through the solid-liquid interface and the vaporization heat, which flows through the liquid-vapor interface.

The results obtained allow one to influence the fluid flow structure in evaporating droplets.

This work was partially supported by the Supercomputing Center of Lomonosov Moscow State University [22].

Appendix A: Numerical method

The calculation of thermal conduction inside the droplet and the substrate is carried out without taking into account the convective heat transfer, which is justified when the inverse Stanton number $St^{-1} = \bar{u}R/\kappa$ is much smaller than

FIG. 4: Temperature distribution inside the droplet and the substrate correspondingly, distribution of absolute value of velocity and vector field plot of velocity for a droplet of 1-hexanol in a three-vortex regime obtained for $\theta = 31.22^\circ$, $k_R = 0.2$, $h_R = 0.1$.

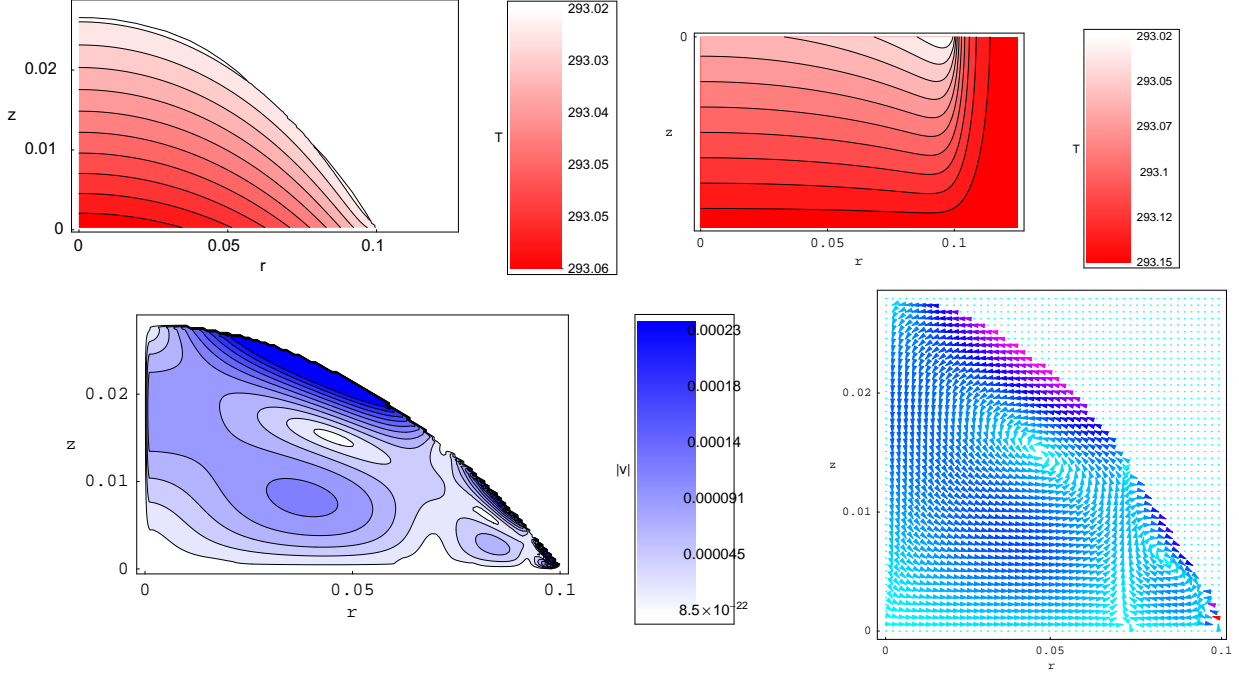
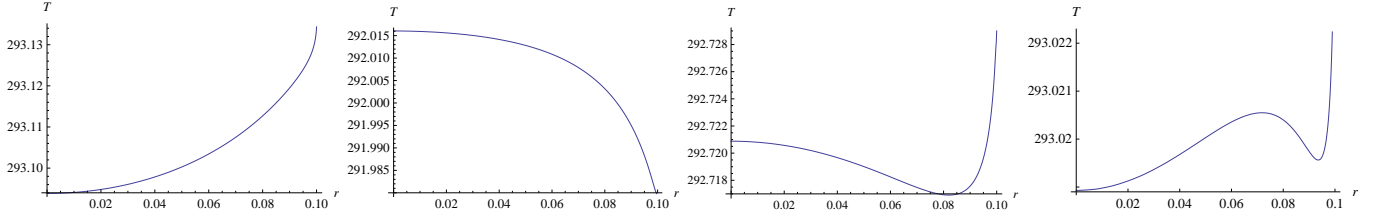


FIG. 5: Surface temperature distribution for a single-vortex, reversed single-vortex, two-vortex and three-vortex regimes corresponding to the 1-hexanol droplets in Figs. 1-4.



unity. The following equation is solved:

$$\frac{\partial T}{\partial t} = \kappa \Delta T. \quad (\text{A1})$$

The boundary conditions for the droplet take the form $\partial T / \partial r = 0$ for $r = 0$; $\partial T / \partial n = -L J_s(r) / k$ at the drop surface. Here \mathbf{n} is a normal vector to the drop surface, J_s is the local evaporation rate determined by $J_s(r) = J_0(\theta)(1 - r^2/R^2)^{-\lambda(\theta)}$, where $\lambda(\theta) = 1/2 - \theta/\pi$ (see [15, 16]), other notations are explained in Table I. The substrate radius is $5R/4$; the substrate thickness is denoted as h_S . At the substrate-fluid interface we have the matching condition $k_S \partial T_S / \partial z = k_L \partial T_L / \partial z$. At the substrate-gas interface we have $\partial T_S / \partial n = 0$, where \mathbf{n} is a normal vector to the substrate surface, since the thermal conductivity of the air is negligibly small. At the bottom of the substrate we have the boundary condition $T_S = T_0$.

In order to accurately take into account the vicinity of the three-phase contact line, which is a very important area of calculation, we have used implicit finite difference method and irregular mesh inside the droplet for the calculation of thermal conduction. We use the following mesh in the drop and the substrate: $r_i = R(1 - (n-i)^2/n^2)$, $i = 0, \dots, n$; $r_i = R(1 + (i-n)^2/n^2)$, $i = n+1, \dots, 3n/2$; $z_j = hj^2/n^2$, $j = 0, \dots, n$, where h is the droplet height and $n = 200$. Inside the substrate, we use the following mesh: $r_{Si} \equiv r_i$, $i = 0, \dots, n$; $z_{Sj} = jh_S/n$, $j = 0, \dots, n$, where h_S is the substrate thickness. Such irregular mesh allows to substantially increase the accuracy of the calculation in the vicinity of the contact line.

We denote the distances between the mesh point (i, j) and its nearest neighbors as $a = r_i - r_{i-1}$, $b = r_{i+1} - r_i$, $c = z_{j+1} - z_j$ and $d = z_j - z_{j-1}$. Then the finite difference representations for the second derivatives are

FIG. 6: Results for θ vs $k_R = k_S/k_L$, where a) $h_R = 0.01$, b) $h_R = 0.05$, c) $h_R = 0.1$, d) $h_R = 0.2$, e) $h_R = 0.5$, f) $h_R = 1$.

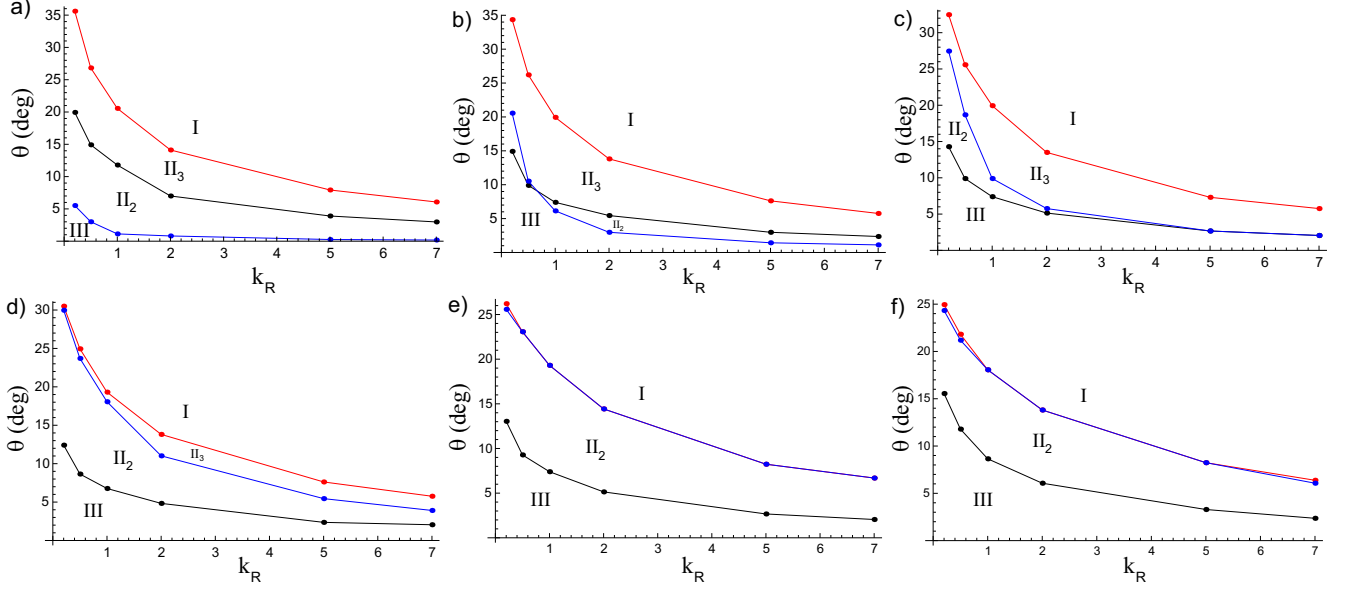
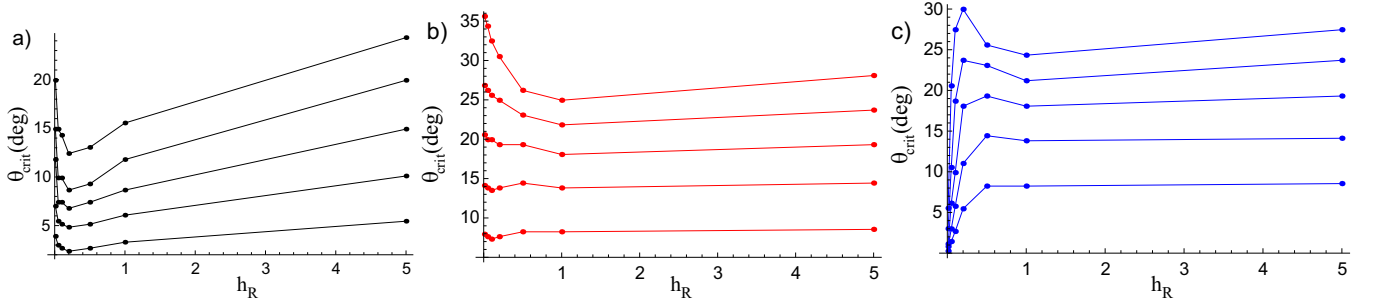


FIG. 7: Dependence of θ_{crit} on $h_R = h_S/R$ for a) the transition corresponding to the change of sign of tangential component of the temperature gradient at the liquid-vapor interface near the contact line; b) the transition to a monotonically increasing surface temperature dependence on r ; c) the transition corresponding to the change of sign of tangential component of the temperature gradient at the liquid-vapor interface near the droplet apex.



$$\hat{\delta}_r^2 T = \frac{2}{(a+b)ab} (aT_{i+1,j}^n - (a+b)T_{ij}^n + bT_{i-1,j}^n), \quad (\text{A2})$$

$$\hat{\delta}_z^2 T = \frac{2}{(c+d)cd} (dT_{i,j+1}^n - (c+d)T_{ij}^n + cT_{i,j-1}^n), \quad (\text{A3})$$

where T_{ij}^n is the temperature at mesh point (i, j) for the n -th time step.

We apply the alternating direction method to Eqn. (A1) with the above notations. In the first part of the method one takes r -derivative implicitly. Then the finite difference representation of Eqn. (A1) is

$$\frac{T_{ij}^{n+1/2} - T_{ij}^n}{\kappa h_t/2} = \hat{\delta}_r^2 T_{ij}^{n+1/2} + \hat{\delta}_z^2 T_{ij}^n + \frac{1}{r} \frac{T_{i+1,j}^{n+1/2} - T_{i-1,j}^{n+1/2}}{a+b}. \quad (\text{A4})$$

For given temperature at time step n it is convenient to rewrite this expression as

$$c'_i T_{i-1,j}^{n+1/2} + (d'_i - 2/(\kappa h_t)) T_{ij}^{n+1/2} + e'_i T_{i+1,j}^{n+1/2} = c''_j T_{i,j-1}^n + (d''_j - 2/(\kappa h_t)) T_{ij}^n + e''_j T_{i,j+1}^n. \quad (\text{A5})$$

TABLE I: The parameter values used in the paper for obtaining the evaporation rates, temperature distribution and hydrodynamics in the drop. The tabular data are taken from [18].

Drop parameters	Initial temperature Contact line radius	$T_0 = 293.15 \text{ K}$ $R = 0.1 \text{ cm}$
Fluid characteristics (1-hexanol)	Density Molar mass Thermal conductivity Thermal diffusivity Dynamic viscosity Surface tension Temperature derivative of surface tension Latent heat of evaporation	$\rho = 0.8136 \text{ g/cm}^3$ $\mu = 102.17 \text{ g/mole}$ $k = 1.5 \cdot 10^{-3} \text{ W/(cm} \cdot \text{K)}$ $\kappa = k/(\rho c_p) = 7.84 \cdot 10^{-4} \text{ cm}^2/\text{s}$ $\eta = 4.578 \cdot 10^{-2} \text{ g/(cm} \cdot \text{s)}$ $\sigma = 25.81 \text{ g/s}^2$ $-\partial\sigma/\partial T = 0.08 \text{ g/(s}^2 \cdot \text{K)}$ $L = 603 \text{ J/g}$
1-hexanol vapor characteristics	Diffusion constant Saturated 1-hexanol vapor density	$D = 0.0621 \text{ cm}^2/\text{s}$ $u_s = 6.55 \cdot 10^{-6} \text{ g/cm}^3$

Here

$$c'_i = 2/((a+b)a) - 1/((a+b)r), \quad d'_i = -2/(ab), \quad e'_i = 2/((a+b)b) + 1/((a+b)r), \quad (\text{A6})$$

$$c''_j = -2/((c+d)d), \quad d''_j = 2/(cd), \quad e''_j = -2/((c+d)c), \quad (\text{A7})$$

$$c'_0 = 0, \quad d'_0 = -4/a^2, \quad e'_0 = 4/a^2, \quad (\text{A8})$$

For each $j \neq 0$ the tridiagonal matrix algorithm is used to solve the set of equations (A5) for the temperature at the time step $n + 1/2$. The boundary interpolation at the droplet surface (see below) and the boundary condition at the substrate-gas interface are solved together with the set of equations (A5) by the tridiagonal matrix algorithm.

In the second part of the method one takes z -derivative implicitly and represents Eqn. (A1) as

$$\frac{T_{ij}^{n+1} - T_{ij}^{n+1/2}}{\kappa h_t/2} = \hat{\delta}_r^2 T_{ij}^{n+1/2} + \hat{\delta}_z^2 T_{ij}^{n+1} + \frac{1}{r} \frac{T_{i+1,j}^{n+1/2} - T_{i-1,j}^{n+1/2}}{a+b}. \quad (\text{A9})$$

For given temperature at time step $n + 1/2$ this expression takes the form

$$c''_j T_{i,j-1}^{n+1} + (d''_j + 2/(\kappa h_t)) T_{ij}^{n+1} + e''_j T_{i,j+1}^{n+1} = c'_i T_{i-1,j}^{n+1/2} + (d'_i + 2/(\kappa h_t)) T_{ij}^{n+1/2} + e'_i T_{i+1,j}^{n+1/2}, \quad (\text{A10})$$

where the coefficients are given in (A6)-(A8). For each i the tridiagonal matrix algorithm is used to solve the set of equations (A10) for the temperature at time step $n + 1$. The boundary condition $T_{S,i0}^{n+1} = T_0$, the boundary interpolation at the droplet surface (see below) and the matching condition $T_{i0} = c_S T_{i1} + c_L T_{S,i,n-1}$ are solved together with the set of equations (A10) by the tridiagonal matrix algorithm, where $c_S = k_L h_{yS}/(k_L h_{yS} + k_S h_{yL})$, $c_L = 1 - c_S$. For $i > n$ the boundary condition at the substrate-gas interface is also used.

At the droplet surface we use the boundary interpolation. Consider a mesh point $D(i, j)$ close to the surface, where $j > 1$. The point D is inside the drop and at least one of its nearest neighbors is outside the drop. In linear approximation $T(r, z) = a + br + cz$ in a vicinity of the point $D(i, j)$. We denote the temperatures at points $D(i, j)$, $B(i-1, j)$ and $C(i, j-1)$ as T_D , T_B and T_C correspondingly; also let $G = \partial T/\partial n = -LJ(r)/k$ at a point A of the drop surface near D . Then one has

$$b \sin \phi + c \cos \phi = G, \quad a + b(i-1)h_r + cjh_z = T_B, \quad a + bjh_r + c(j-1)h_z = T_C. \quad (\text{A11})$$

The solution of the set of equations is

$$a = (h_r \cos \phi (iT_B - (i-1)T_C) + h_z \sin \phi (T_B + j(T_C - T_B)) - h_r h_z G (j+i-1)) / R \quad (\text{A12})$$

$$b = (h_z G + (T_C - T_B) \cos \phi) / R \quad (\text{A13})$$

$$c = (h_r G + (T_B - T_C) \sin \phi) / R \quad (\text{A14})$$

$$R = h_r \cos \phi + h_z \sin \phi. \quad (\text{A15})$$

In the first part of the alternating direction method the calculations of rows proceed towards larger values of j . For this reason one should consider here T_C and G as given quantities, whereas T_B and T_D are unknown. It is convenient

under these conditions to represent (A12)-(A15) as

$$a = a_0 + a_1 T_B, \quad b = b_0 + b_1 T_B, \quad c = c_0 + c_1 T_B, \quad (\text{A16})$$

and obtain explicit expressions for $a_0, a_1, b_0, b_1, c_0, c_1$. This results in linear relation between T_D and T_B

$$T_D = a + b r_D + c z_D = (a_0 + b_0 r_D + c_0 z_D) + (a_1 + b_1 r_D + c_1 z_D) T_B, \quad (\text{A17})$$

which can be transformed to the form $d'_{i-1} T_{i-1,j}^{n+1/2} + e'_{i-1} T_{ij}^{n+1/2} = b'_{i-1}$. This completes the set of equations (A5) for the tridiagonal matrix algorithm. Here $d'_{i-1} = -(a_1 + b_1 r_D + c_1 z_D)$, $e'_{i-1} = 1$, $b'_{i-1} = a_0 + b_0 r_D + c_0 z_D$.

To carry out the boundary interpolation in the second part of the alternating direction method, similar expressions can be derived to relate T_D and T_C . A similar boundary interpolation method is also derived for $j \leq 1$.

-
- [1] H.Y. Erbil, Evaporation of pure liquid sessile and spherical suspended drops: A review, *Adv. Colloid Int. Sci.* **170**, 67 (2012).
 - [2] R.G. Larson, Transport and deposition patterns in drying sessile droplets, *AIChE Journal* **60**(5), 1538 (2014).
 - [3] D. N. Voylov, L. M. Nikolenko, D. Yu. Nikolenko, N. A. Voylova, E. M. Olsen, V. F. Razumov, Self-Assembly of charged CdTe nanoparticles, *JETP Letters* **95**(12), 656 (2012).
 - [4] Z. L. Wang, Structural analysis of self-assembling nanocrystal superlattices, *Adv. Mater.* **10**, 13 (1998).
 - [5] G. Ge, L. Brus, Evidence for spinodal phase separation in two-dimensional nanocrystal self-assembly, *J. Phys. Chem. B* **104**, 9573 (2000).
 - [6] Y. Cai, B. Z. Newby, Marangoni flow-induced self-assembly of hexagonal and stripelike nanoparticle patterns, *J. Am. Chem. Soc.* **130**, 6076 (2008).
 - [7] S. Narayanan, J. Wang, X. M. Lin, Dynamical self-assembly of nanocrystal superlattices during colloidal droplet evaporation by in situ small angle x-ray scattering, *Phys. Rev. Lett.* **93**, 135503 (2004).
 - [8] T. P. Bigioni, X. M. Lin, T. T. Nguyen, E. I. Corwin, T. A. Witten, H. M. Jaeger, Kinetically driven self assembly of highly ordered nanoparticle monolayers, *Nature Materials* **5**, 265 (2006).
 - [9] H. Hu, R. G. Larson, Analysis of the Effects of Marangoni Stresses on the Microflow in an Evaporating Sessile Droplet, *Langmuir* **21**, 3972 (2005).
 - [10] W. D. Ristenpart, P. G. Kim, C. Domingues, J. Wan, H. A. Stone, Influence of substrate conductivity on circulation reversal in evaporating drops, *Phys. Rev. Lett.* **99**, 234502 (2007).
 - [11] X. Xu, J. Luo, D. Guo, Criterion for Reversal of Thermal Marangoni Flow in Drying Drops, *Langmuir* **26**(3), 1918 (2010).
 - [12] L.Yu. Barash, Dependence of the fluid convection in an evaporating sessile droplet on the thermal conductivity of the substrate, XXIII IUPAP Conference on Computational Physics (2011), http://ccp2011.ornl.gov/pdf/Abstracts/Barash_Lev_9.1b_8.pdf
 - [13] K. Zhang, L. Ma, X. Xu, J. Luo, D. Guo, Temperature distribution along the surface of evaporating droplets, *Phys. Rev. E* **89**, 032404 (2014).
 - [14] L.Yu. Barash, T.P. Bigioni, V.M. Vinokur, L.N. Shchur, Evaporation and fluid dynamics of a sessile drop of capillary size, *Phys. Rev. E* **79**, 046301 (2009).
 - [15] R. D. Deegan, O. Bakajin, T. F. Dupont, G. Huber, S. R. Nagel, T. A. Witten, Contact line deposits in an evaporating drop, *Phys. Rev. E* **62**, 756 (2000).
 - [16] H. Hu, R. G. Larson, Evaporation of a Sessile Droplet on a Substrate, *J. Phys. Chem. B* **106**, 1334 (2002).
 - [17] H. Hu, R. G. Larson, Analysis of the Microfluid Flow in an Evaporating Sessile Droplet, *Langmuir* **21**, 3963 (2005).
 - [18] D. R. Lide, *CRC Handbook of Chemistry and Physics* (CRC Press, 2004).
 - [19] J. R. A. Pearson, On convection cells induced by surface tension, *J. Fluid Mech.* **4**, 489 (1958).
 - [20] F. Duan, V. K. Badam, F. Durst, C. A. Ward, Thermocapillary transport of energy during water evaporation, *Phys. Rev. E* **72**, 056303 (2005).
 - [21] N. Murisic and L. Kondic, On evaporation of sessile drops with moving contact lines, *J. Fluid Mech.* **679**, 219 (2011).
 - [22] Voevodin V.I., Zhumaty S.A., Sobolev S.I., Antonov A.S., Bryzgalov P.A., Nikitenko D.A., Stefanov K.S., Voevodin V.I., Practice of "Lomonosov" Supercomputer, *Open Systems J.*, Moscow: Open Systems Publ., 2012, no.7. (In Russian)